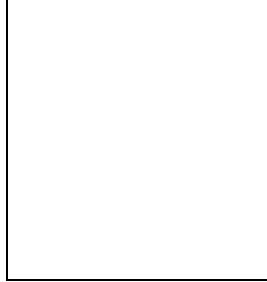


Soft Particle Spectra at STAR

Zhangbu Xu for the STAR Collaboration
Department of Physics, Building 510a, P.O. Box 5000,
Upton, NY 11973



We presented the multiplicity and the spectra of many particles in Au+Au at $\sqrt{s_{NN}} = 130$ GeV measured by STAR detector. Their connections to initial condition, baryon creation, freeze-out condition and strangeness enhancement were discussed.

In relativistic heavy ion collisions at RHIC, thousands of particles of different properties are created. Although interactions with very high momentum transfer can be more easily calculated using perturbative QCD, the dominant interactions in these collisions happen at low momentum transfer. The bulk of the system may go through a phase transition from ordinary hadronic matter to hot and dense Quark-Gluon Plasma (QGP). To address this issue about whether a phase transition to QGP happens from measurements of soft particle spectra, we would like to know what the initial conditions are, whether the system is thermalized, whether the gluon degree of freedom dominates at certain stage, how long it takes for the system to evolve from one stage to another stage.

We report the charged particle multiplicity, the mean transverse momentum (p_T) and its centrality dependence, the particle transverse momentum spectra of many particles ($\pi^\pm, K^\pm, K_S^0, K^*, \phi, p, \bar{p}, \Lambda, \bar{\Lambda}, \Xi, \bar{\Xi}, \bar{d}, \bar{3}He$, etc.) and their centrality dependence measured by STAR detector at RHIC. Based on these measurements, we discussed the mean p_T scaling in the context of gluon saturation model, the strangeness enhancement ($\bar{\Lambda}/\bar{p}, K/\pi, \phi/K^*(892)^0$), radial flow (mass dependence of m_T slope), the fitted results of statistical model and coalescence model on baryon chemical potential (μ_B) and temperature (T) and the time scale of the evolution of the system ($K^*(892)^0/K$).

The detector system used for these studies was the Solenoidal Tracker at RHIC (STAR). The main tracking device within STAR is the Time Projection Chamber (TPC) which is used to provide momentum information and particle identification for charged particles by measuring their ionization energy loss (dE/dx). A minimum bias trigger was defined using coincidences between two Zero Degree Calorimeters (ZDC) which measured the spectator neutrons. A Central Trigger Barrel (CTB) constructed of scintillator paddles surrounding the TPC was used to select small impact parameter “central” collisions by selecting events with high charged particle multiplicity. Data were taken for Au+Au collisions at $\sqrt{s_{NN}} = 130$ GeV in the summer of 2000.

STAR measured charge multiplicity per unit of pseudorapidity (η) for the 5% most central collisions¹. The negatively charged hadron multiplicity and its mean p_T are $dN/d\eta|_{|\eta|<0.5} = 567 \pm 1 \pm 38$ and $\langle p_T \rangle = 0.508 \pm 0.012$ GeV/ c . The multiplicity per participant pairs increases by 38% relative to $p\bar{p}$ and 52% compared to nuclear collisions at $\sqrt{s_{NN}} = 17$ GeV. The $\langle p_T \rangle$ increases by 30% and 18% respectively from 0.392 GeV/ c in $p\bar{p}$ collisions and $\simeq 0.429$ GeV/ c

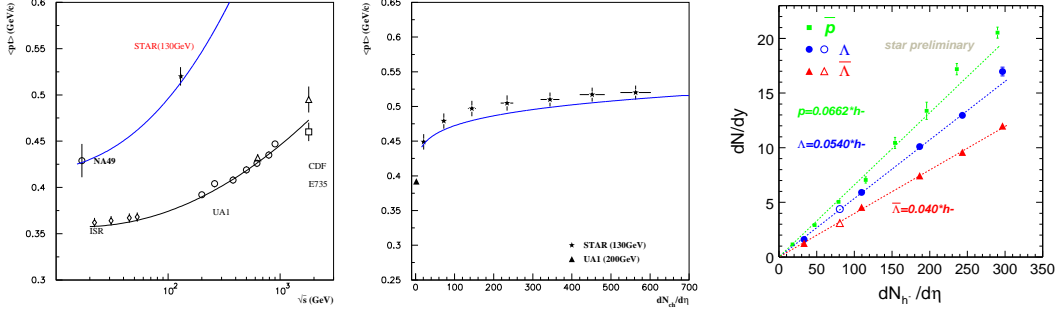


Figure 1: Left: mean p_T of h^- , N_{ch} as a function of $\sqrt{s_{NN}}$ for pp , $\bar{p}p$ and central AA collisions. Right: mean p_T of N_{ch} as a function of N_{ch} at $\sqrt{s_{NN}} = 130$ GeV. Curves are from Eq.1.

Figure 2: dN/dy of \bar{p} , Λ , $\bar{\Lambda}$ as a function of h^- . Linear dependence can describe the data well.

in Pb+Pb collisions at SPS^{1,2}. The left panel of Fig. 1 shows mean p_T of h^- or N_{ch} as a function of $\sqrt{s_{NN}}$ for pp , $\bar{p}p$, AA collisions. $\langle p_T \rangle_{pp} = 0.40 - 0.03 \times \ln x + 0.0053 \times (\ln x)^2$ is a parametrization of the measured mean p_T in pp collisions⁵ as shown in the plot. Both gluon saturation³ and hydrodynamics⁴ predict some scaling behavior of $\langle p_T \rangle \sim \sqrt{(\frac{dN}{d\eta})_{AA}/\pi R^2}$ when conditions are satisfied. To get a quantitative analysis on the dependence between $\langle p_T \rangle$ and multiplicity, we require that the scaling dependence is linear and it should also satisfy the pp results. By doing this, there is only one free parameter as shown in Eq. 1.

$$\langle p_T \rangle_{AA} = a + \sqrt{\frac{s_{AA}}{s_{pp}}} (\langle p_T \rangle_{pp} - a), \quad (1)$$

where $s_{AA} = (\frac{dN}{d\eta})_{AA}/\pi R^2$ and $s_{pp} = (\frac{dN}{d\eta})_{pp}/\pi r_0^2$ are the multiplicity density per unit pseudorapidity per unit transverse area in AA and pp collisions ($R = r_0 A^{1/3}$) and $a = 0.3$ GeV/ c is a constant chosen to describe the AA data. For non-central collisions, calculation of the transverse area is not as straight forward. We take the parametrization of the centrality dependence of s_{AA} from Ref.³. The solid curves in Fig. 1 show the energy dependence and centrality dependence of $\langle p_T \rangle$ from Eq. 1. The curves describe the data well. It will be interesting to see if the description holds with an energy scan from lower energy to highest energy at RHIC.

Strangeness enhancement has long been predicted to be a possible signature of QGP⁶. The measurements of kaon, Λ , ϕ , Ξ , Ω and their antiparticles have been under way with the STAR detector. Measurements of antihyperon to antiproton ratio ($\bar{\Lambda}/\bar{p}$) at lower energies indicate large enhancement of this ratio in AA collisions when compared to pp collisions⁷. The interpretation of the results is complicated by the fact that the antimatter absorption in a baryon rich environment is significant or even dominant at lower beam energies⁸. At RHIC, the \bar{p}/p ratio is approaching unit indicating low net baryon density⁹. Both \bar{p} and $\bar{\Lambda}$ were measured at STAR with high statistics^{9,10} as shown in Fig. 2. Antiprotons which include feeddown from $\bar{\Lambda}$ decays are identified by the ionization energy loss (dE/dx) when particles traverse the TPC. Antilambdas are identified by their decay topology and mixed-event method. The integrated yields of dN/dy at $y = 0$ of the three particles are approximately proportional to the $dN_{h^-}/d\eta$. This means that there is very little centrality dependence of \bar{p}/π and $\bar{\Lambda}/\bar{p}$ which is very different from AGS and SPS results^{7,11}. Our result of $\bar{\Lambda}/\bar{p} = 0.93_{-0.23}^{+0.57}$ after feeddown correction^{9,10} for both $\bar{\Lambda}$ and \bar{p} in central Au+Au collisions shows significant increase from elementary collisions. It has been speculated that the enhancement seen in pA and AA collisions may be related to number of collisions¹² or the degree of violence of the collisions (characterized by charge multiplicity)¹³. An alternative explanation is that strangeness is in equilibrium with the rest of the particles in the system since the thermal/statistical models describe the data well at RHIC^{14,15}.

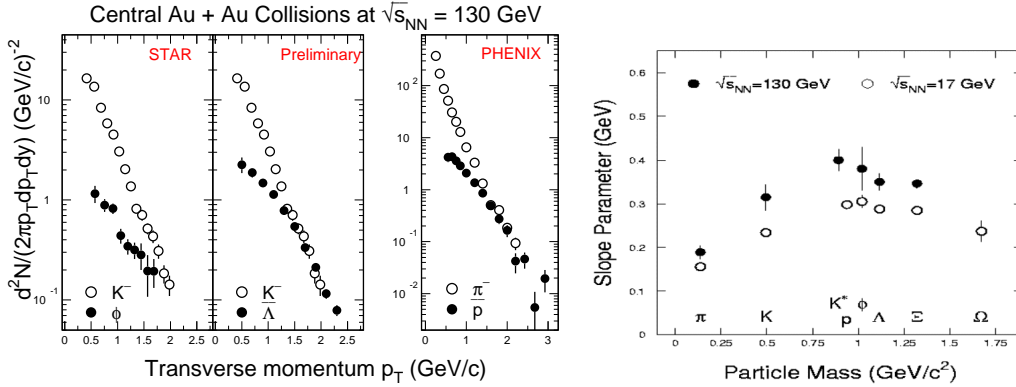


Figure 3: Left: p_T spectra of pseudoscalar and vector meson, hyperon and strange meson, baryon and meson. Right: Inverse slope of the transverse spectra vs mass of the particle. The errors are statistical only. The systematical uncertainty of STAR data is 10-15% depending on particles.

In addition, K/π and ϕ/K^{*0} measured at STAR¹⁶ also indicate enhancement in AA collisions relative to elementary collisions.

The detailed p_T spectra of identified particles carry information about the radial flow and temperature of the system^{15,17}. Fig. 3 (left panel) shows p_T spectra of pseudoscalar and vector meson, hyperon and strange meson, baryon and meson. They exhibit a common feature that the production of heavy particle decreases much slower than that of lighter particle with increasing p_T . At $p_T \simeq 2$ GeV/c, there are as many heavy particles produced as the lighter particles. This can be explained by the radial flow where all particles have same temperature and a common flow velocity¹⁵. Fig. 3 (right panel) shows the inverse slope parameters of p_T spectra as a function of particle mass. It has been seen that heavier particles have larger flow effect. In fact, thermal model with radial flow can extract the temperature and flow velocity at kinetic freeze-out from the p_T spectra at RHIC. There is also a novel mechanism proposed to explain the p/π ratio¹⁸.

One of the unknowns of particle production in strong interaction is the probability that a quark and antiquark pair produces a vector meson as compared to its pseudoscalar partner. It is thus important to measure the vector mesons and pseudoscalar mesons to understand the production mechanism involving spin in strong interactions under extreme conditions. We have measured the $K^*(892)^0$ and $\bar{K}^*(892)^0$ in relativistic nucleus-nucleus collisions¹⁹ as shown in Fig. 4. The K^{*0} m_T spectrum from the 14% most central Au+Au collisions results in an inverse slope parameter of $0.40 \pm 0.02 \pm 0.04$ GeV, similar to that measured for the ϕ meson using a similar centrality cut¹⁶. The measured yield, $dN/dy = 10.0 \pm 0.9(\text{stat}) \pm 2.5(\text{sys})$ is relatively high compared to elementary collisions and thermal model predictions, considering the short K^{*0} lifetime ($c\tau \simeq 4$ fm) and expected losses due to rescattering of the decay daughters in the dense medium¹⁹.

The measurements of nuclei and antinuclei production are sensitive to the volume and nucleon and antinucleon phase space density at the freeze-out because the nuclei are believed to be produced via coalescence of nucleons²⁰. Due to secondary nuclei production from beam pipe and limited p_T range of PID from dE/dx , STAR is only able to identify and measure light antinuclei (\bar{d} , $\bar{^3He}$), \bar{p} and proton. Fig. 5 shows the measured differential yield at $p_T/A \simeq 0.4$ GeV/c as function of particle's atomic number A for p , \bar{p} , \bar{d} , $\bar{^3He}$. Using a simplified formulae $\frac{dN}{p_T dp_T dy} \propto \exp(-(m_B \pm \mu_B)A/T)$ from Ref.²¹, we are able to fit well the nucleus production at low p_T at AGS²², SPS²³ and RHIC heavy ion collisions and obtain temperature and baryon chemical potential at kinetic freeze-out. The results are: $T = 126$ MeV, $\mu_B = 21$ MeV (RHIC); $T = 130$ MeV, $\mu_B = 170$ MeV (SPS); $T = 110$ MeV, $\mu_B = 500$ MeV (AGS). Errors were esti-

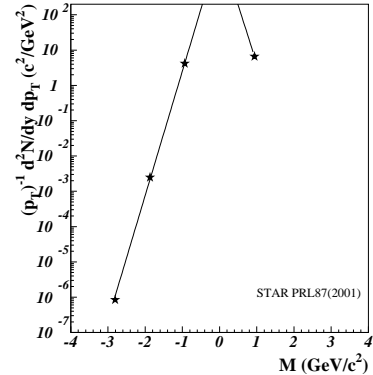
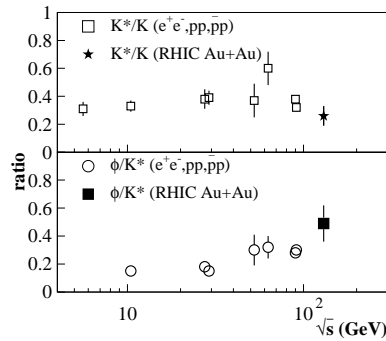
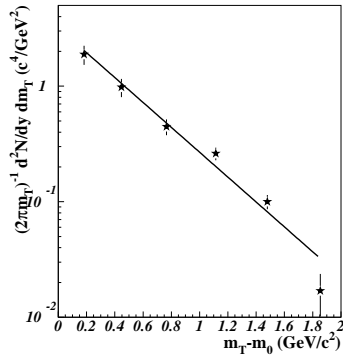


Figure 4: Left: m_T spectrum of K^{*0} in 14% most central Au+Au collisions. Right: K^{*0}/K and ϕ/K^{*0} ratios vs beam energy in elementary collisions and central Au+Au collisions.

Figure 5: The measured differential yield at $p_T \simeq 0.4$ GeV/c as function of particle's atomic number A for $p, \bar{p}, d, \bar{d}, {}^3\text{He}$.

ated to be ± 10 MeV for all the cases²². The ratios of μ_B/T at kinetic freeze-out vs that at chemical freeze-out at AGS, SPS and RHIC central AA collisions¹⁴ are consistent with each other even though the parameters at chemical freeze-out are extracted from thermal fit to the many ratios of the integrated particle yields while the parameters from coalescence are from nuclear cluster formation rate at low p_T . However, further study is needed to see if such a trajectory in the phase diagram is possible²⁴.

In summary, we report recent results from the STAR experiment: i) Charged particle multiplicity and their averaged values of transverse momentum are discussed within the framework of both gluon saturation and hydrodynamic models; ii) The identified particle distributions provided information on both chemical equilibrium and collective expansion; iii) Resonances and light nuclei formation may provide a probe of the evolution of the system at late stage of the collision. In order to determine the formation of a system with partonic degree of freedom, we need to systematically measure the spectra of all the particles listed and new particles (especially multistrange and heavy-flavor particles) at different beam energies and beam species.

References

1. C. Adler *et al.*, *Phys. Rev. Lett.* **87**, 112303 (2001); C. Adler *et al.*, nucl-ex/0206011.
2. H. Appelschauser *et al.*, *Phys. Rev. Lett.* **82**, 2471 (1999).
3. L. McLerran *et al.*, *Phys. Lett. B* **514**, 29 (2001); J. Schaffner-Bielich *et al.*, nucl-th/0202054.
4. D. K. Srivastava, *Phys. Rev. C* **64**, 064901 (2001).
5. C. Albajar *et al.*, *Nucl. Phys. B* **335**, 261 (1990).
6. J. Rafelski and B. Mueller, *Phys. Rev. Lett.* **48**, 1066 (1982); **56** 2334E, (1986).
7. B.B. Back *et al.*, *ibidem* **87**, 242301 (2001); T.A. Armstrong *et al.*, *Phys. Rev. C* **59**, 2699 (1999).
8. F.Q. Wang, *J. Phys. G* **27**, 283 (2001).
9. C. Adler *et al.*, *Phys. Rev. Lett.* **86**, 4778 (2001); C. Adler *et al.*, *ibidem* **87**, 262302 (2001).
10. C. Adler *et al.*, nucl-ex/0203016.
11. I.G. Bearden *et al.* nucl-ex/0202019.
12. I. Chemakin *et al.* *Phys. Rev. Lett.* **85**, 4868 (2000).
13. G. Bocquet *et al.* *Phys. Lett. B* **366**, 441 (1996).
14. P. Braun-Munzinger *et al.* *Phys. Lett. B* **518**, 41 (2001); D. Magestro *J. Phys. G* **28**, 1745 (2002);
15. N. Xu and M. Kaneta, *Nucl. Phys. A* **698**, 306c (2002).
16. C. Adler *et al.*, nucl-ex/0206008; C. Adler *et al.*, *Phys. Rev. C* **65**, 041901(R) (2002).
17. D. Teaney, *et al.*, nucl-th/0110037.
18. I. Vitev and M. Gyulassy, hep-ph/0108045.
19. C. Adler *et al.*, nucl-ex/0205015.
20. C. Adler *et al.*, *Phys. Rev. Lett.* **87**, 262301 (2001).
21. R. Scheibl, U. Heinz, *Phys. Rev. C* **59**, 1585 (1999).
22. Z. Xu *et al.*, nucl-ex/9909012.
23. G. Ambrosini *et al.*, nucl-ex/0011016.
24. R. Rapp, hep-ph/0204131.